

Leveraging Image Matching Toward End-to-End Relative Camera Pose Regression

Fadi Khatib*

Yuval Margalit*

Meirav Galun

Ronen Basri

Weizmann Institute of Science

Abstract

This paper proposes a generalizable, end-to-end deep learning-based method for relative pose regression between two images. Given two images of the same scene captured from different viewpoints, our method predicts the relative rotation and translation (including direction and scale) between the two respective cameras. Inspired by the classical pipeline, our method leverages Image Matching (IM) as a pre-trained task for relative pose regression. Specifically, we use LoFTR, an architecture that utilizes an attention-based network pre-trained on Scannet, to extract semi-dense feature maps, which are then warped and fed into a pose regression network. Notably, we use a loss function that utilizes separate terms to account for the translation direction and scale. We believe such a separation is important because translation direction is determined by point correspondences while the scale is inferred from prior on shape sizes. Our ablations further support this choice. We evaluate our method on several datasets and show that it outperforms previous end-to-end methods. The method also generalizes well to unseen datasets.

1. Introduction

Computing the relative pose (position and orientation) between two cameras given an image pair is a fundamental computer vision task and an essential step in multiview structure from motion (SfM) pipelines [39, 51, 52, 63, 64], with applications to autonomous robot navigation and to virtual and augmented reality. Classical techniques rely on keypoint extraction and matching using descriptors such as SIFT [8, 15, 36, 48, 49], followed by robust estimation of the essential matrix using, e.g., RANSAC [23]. These methods can recover the relative pose very accurately. However, (1) they only recover five of the six degrees of freedom of the relative pose; the distance between the two camera

positions cannot be recovered from point correspondences; (2) RANSAC generally requires many iterations (faster versions were recently proposed, e.g., MAGSAC++ [6]), and (3) classical methods are sensitive to matching errors due to the presence of repetitive structures or lighting differences.

To overcome these drawbacks, a number of recent papers have explored the use of deep neural networks for relative pose regression (RPR). While some methods replaced only parts of the pipeline (e.g., the keypoint extraction and matching, see Section 2 for discussion), our focus is on end-to-end RPR network solutions. These new RPR methods use appearance and pose priors to guide the matching of point features and to select the likely relative pose given an input image pair. In particular, deep methods can recover the distance between two cameras by exploiting priors on the size of the observed objects. Nevertheless, current deep methods are not yet as accurate as the classical approach in many settings [7, 29, 30]. Moreover, existing methods still struggle with cross-scene/dataset generalization.

Below we propose a three-step, deep network architecture for relative pose regression (see architecture in Figure 1). Similar to the classical techniques, our network proceeds by first computing feature descriptors for each image, then matching these features across the two images and finally regressing the motion parameters. For the first step we compute for each image a semi-dense feature map using the pre-trained LoFTR architecture [53]. The second step matches and warps the most similar feature in the second image to each feature in the first image. The final step uses a residual network to compute the pose from the warped features.

We only train the last step in this pipeline. For training, we use a modified loss, compared to previous work [3, 31, 47]. Noticing that translation direction is determined by the point matches, whereas the scale of translation is determined by a prior on the object size, we separate these in the loss: we use a cosine similarity term to train for direction and an ℓ_1 term to train for scale. An additional term is used to train for orientation. We balance these terms simply and uniformly with the constant 1 and explore a similar, three-head architecture that requires no balancing of terms.

*Equal contributors.

Project webpage:

<https://fadikhatib.github.io/GRelPose>

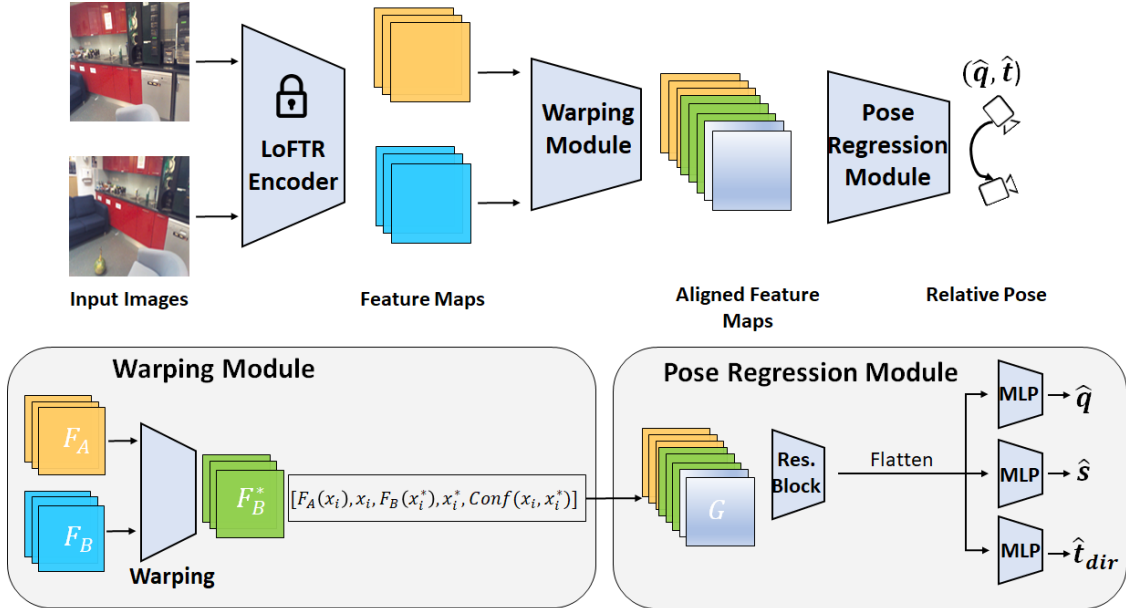


Figure 1. **Network architecture.** Our network is composed of three modules (top), LoFTR which given an image pair produces a coarse grid of features, a warping module, and a pose regression module. The bottom figure shows a detailed description of the warping and pose regression modules.

The main contributions of our work are as follows. (1) We leverage IM as a pre-training task for relative pose regression, offering a novel perspective on end-to-end relative pose estimation. (2) Unlike the previous works, our loss treats separately the direction and scale of the camera position vector, using the cosine similarity for the directional loss and an ℓ_1 loss for the scale. (3) We use hard matching and warping, instead of soft matching and warping as in [3], we show empirically the advantage of our choice. (4) We validate that our pre-trained IM backbone generates effective feature representations for RPRs, highlighting also the contribution of interleaved self- and cross-attention modules in capturing feature similarities across image pairs. (5) We test our method on various datasets, including cases in which the training and test datasets differ (e.g., training on indoor scenes and testing on outdoor scenes). Our method achieves superior results to other end-to-end RPR networks in nearly all experiments. (6) Our method has made significant advancement in closing the performance gap between RPRs and feature matching methods, while maintaining substantially faster inference time.

2. Related Work

Relative Pose Estimation. The pose between two images with known intrinsic parameters can be recovered by decomposing the essential matrix [25], yielding a relative rotation and a scaleless translation direction vector. The essential matrix is classically estimated by matching local fea-

tures, such as [8, 15, 36, 48, 49], followed by a numerical scheme, e.g., the 5-point solver [38] inside robust estimator loop, namely RANSAC [23] and others [5, 6, 41]. Despite the success of this classical approach, it lacks the ability to utilize priors, for example, to infer the unknown distance between the two cameras. These shortcomings have led to the introduction of deep-based approaches, which we review next.

Deep feature extraction and matching. Several studies have utilized deep networks to detect and match point features in image pairs [9, 21, 28, 45, 50, 53, 55–57, 60, 65]. Among these, LIFT [65] is an early approach that additionally assigns an orientation to each feature. SuperGlue [50] uses a Graph Neural Network (GNN) to match two sets of interest points. Lightglue [34] uses self and cross attention alongside key-point pruning and early adaptive depth mechanism to improve on SuperGlue’s inference speed and accuracy, utilizing keypoints and descriptors extracted, for example, with SuperPoint[19]. A number of works utilize neural networks to construct a differentiable matching module (providing also matching confidence) [55–57]. The recent LoFTR [53] and COTR [28] utilize self- and cross-attention layers along with multiscale analysis to produce semi-dense, near-pixel-wise correspondences. The relative pose is then obtained by applying RANSAC to the extracted correspondences. Those methods were shown to produce accurate correspondences even in low-texture areas, demonstrating good generalization ability across scenes and datasets. Still, those methods are not

end-to-end approaches, and the relative position is recovered up to a scale factor.

Deep RANSAC. Recent works sought to construct a deep network architecture that can robustly estimate the essential matrix from point matches. Specifically, DSAC [13] replaces RANSAC’s hypothesis selection with a robust average of hypotheses, resulting in a differentiable counterpart of RANSAC. [14] suggests using a fixed backbone for the DSAC* network and training only a scene-specific regression head. Alongside a novel training loss, it resulted in faster convergence and better accuracy. [17] utilizes convolutions in high dimension to recover the essential matrix robustly. [10, 11, 42] propose a deep-based scheme to distinguish between inliers and outliers, given putative correspondences, for the tasks of fundamental matrix estimation and camera re-localization.

End-to-end relative pose regression (RPR). A number of deep learning methods attempt to predict the relative pose directly from input image pairs, circumventing the need to detect 2D putative matches explicitly. Early works [31, 37] used ResNet34 pre-trained for classification on the Imagenet dataset to produce holistic feature embeddings that describe the two input images. An MLP module was then applied to these feature vectors to regress the relative position, with its magnitude, as well as the relative orientation. Subsequent works [1, 4, 22, 62, 68] utilized a similar approach using modified loss functions and architectures. All of these methods have limited cross-scene generalization ability. Recent works [32, 67] have utilized energy-based relative pose models for multi-view pose estimation, demonstrating their efficacy in sparse object-centric scenarios exemplified by the CO3D dataset [44]. Their applicability to more general scenes, however, remains a challenge.

Recently, [47] advocated the use of Vision Transformer (ViT) feature maps [20, 61] for relative pose regression. They further incorporated quadratic positional encoding to produce an architecture that mimics the Eight-Point Algorithm for essential matrix recovery [26]. Lastly, The Map-free benchmark [3] suggests baselines with different output parametrizations for RPR, using a residual UNet (ResUNet) architecture to produce a feature map for each image. A soft feature matching was obtained by computing a 4D correlation volume followed by softmax. This soft matching was then used to warp the features of one image into their corresponding locations in the other image. A regression module was finally used to estimate the relative pose.

3. Method

Our goal, given two images of a scene captured from different viewpoints, is to predict the relative position and orientation between the two respective cameras, including the distance between their centers. Similar to recent approaches to end-to-end RPR networks [3, 47], we use a three-module

architecture (see Fig. 1), a frozen feature extraction module, a matching and warping module, and a pose regression head. Our architecture improves over previous work by relying on the powerful LoFTR IM architecture [53] to produce a semi-dense feature map, warping the feature maps by utilizing hard matches between the produced features, followed by a camera motion regressor, which is trained by a loss in which translation direction and scale are separated into different terms. These modifications allow us to significantly improve accuracy and achieve cross-scene and cross-dataset generalization. Below we describe the three modules and our loss function.

3.1. Feature extraction

For feature extraction we use the coarse module of LoFTR [53], which is pre-trained for matching on the Scannet dataset [18], depicting indoor scenes. We keep the weights of this module frozen throughout the training of our network. The LoFTR architecture is applied to both images in parallel. Denote the input images by I_A and I_B . Each image is first fed to a feature pyramid network [33], producing a pixel-wise feature map at the desired resolution. Next, a positional encoding is summed to these maps. The obtained maps are then fed into a sequence of interleaved self- and cross-attention layers, producing the final feature maps, $F_A(\mathbf{x}_i), F_B(\mathbf{x}_j) \in \mathbb{R}^C$, where C denotes the number of feature channels, $1 \leq i, j \leq n, n = WH/64$, and W and H denote the width and height of the input images in their original resolution. Note that, unlike in [3], the cross-attention steps modify the feature maps to account for the features seen in the other image, potentially encouraging their matching.

3.2. Matching and warping

Our next aim is to identify matching points. Given the coarse feature maps $F_A(\mathbf{x}_i)$ and $F_B(\mathbf{x}_j)$ (expressed as column vectors), we select for each point \mathbf{x}_i in I_A a corresponding point \mathbf{x}_i^* in I_B by maximizing the correlation between their respective feature vectors, $F_A(\mathbf{x}_i)$ and $F_B(\mathbf{x}_i^*)$. Specifically, the coordinate \mathbf{x}_i^* in I_B is determined by

$$\mathbf{x}_i^* = \underset{j}{\operatorname{argmax}}(F_A^T(\mathbf{x}_i)F_B(\mathbf{x}_j)). \quad (1)$$

Additionally, we use the computed correlations $F_A^T F_B$ to calculate a confidence score by applying softmax over each collection of correlations for point \mathbf{x}_i in the first image, namely,

$$\operatorname{conf}(\mathbf{x}_i, \mathbf{x}_i^*) = \max(\operatorname{softmax}(F_A^T(\mathbf{x}_i)F_B(\mathbf{x}_j))). \quad (2)$$

Next, we concatenate corresponding features, append an encoding of their positions in the two images, and the confidence score, obtaining a feature map of correspondences,

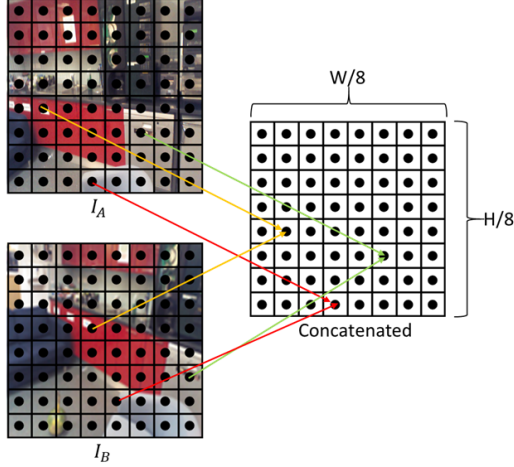


Figure 2. **The warped feature map.** Given a feature vector from Image A, we compute the dot product with all feature vectors in Image B, and we use it to warp the features in F_B their corresponding features in F_A , see (1).

namely,

$$G(\mathbf{x}_i) = [F_A^T(\mathbf{x}_i), \mathbf{x}_i, F_B^T(\mathbf{x}_i^*), \mathbf{x}_i^*, \text{conf}(\mathbf{x}_i, \mathbf{x}_i^*)]. \quad (3)$$

Note that in this feature map, the features in F_B are warped to their corresponding features in F_A (see Fig. 2).

3.3. Pose Regression module

Given the warped feature map, $G(\mathbf{x}_i)$, we apply a sequence of residual blocks followed by an MLP that regresses the different components of the relative pose, $(\hat{\mathbf{q}}, \hat{\mathbf{t}}_{dir}, \hat{s}) \in \mathbb{R}^8$, where $\hat{\mathbf{q}} \in \mathbb{R}^4$ denotes the predicted rotation represented as a quaternion, $\hat{\mathbf{t}}_{dir} \in \mathbb{R}^3$ denotes the signed direction of the translation, and \hat{s} is a scalar, denoting the scale of the translation. The quaternion $\hat{\mathbf{q}}$ and translation direction $\hat{\mathbf{t}}_{dir}$ are normalized to unit magnitude to respectively depict a rotation and an orientation.

3.4. Loss Function

We use supervised learning to train the pose regression module. Given image pairs with ground truth pose specified by a rotation quaternion \mathbf{q} and position \mathbf{t} , we let

$$\mathcal{L}_q(I_A, I_B) = \left\| \frac{\hat{\mathbf{q}}}{\|\hat{\mathbf{q}}\|} - \mathbf{q} \right\|_1, \quad (4)$$

$$\mathcal{L}_{t_{dir}}(I_A, I_B) = 1 - \frac{\langle \hat{\mathbf{t}}_{dir}, \mathbf{t} \rangle}{\|\hat{\mathbf{t}}_{dir}\| \|\mathbf{t}\|}, \quad (5)$$

and

$$\mathcal{L}_s(I_A, I_B) = |\hat{s} - \|\mathbf{t}\||, \quad (6)$$

where \mathcal{L}_q measures the rotation error $\mathcal{L}_{t_{dir}}$ depicts the direction error of the translation, and \mathcal{L}_s depicts the metric error in the translation. A quaternion \mathbf{q} has the form

$(\cos(\theta/2), \mathbf{v} \sin(\theta/2))$, where θ represents a rotation angle and \mathbf{v} represents an axis of rotation. This means that $\pm \mathbf{q}$ represents the same rotation; therefore, to avoid ambiguity, we set its first entry in the ground truth annotation to be positive.

As [29] shows, balancing rotation and translation terms can be challenging. Here we simply assign equal weights to each term in the loss, i.e.,

$$\mathcal{L}(I_A, I_B) = \mathcal{L}_q(I_A, I_B) + \mathcal{L}_{t_{dir}}(I_A, I_B) + \mathcal{L}_s(I_A, I_B). \quad (7)$$

Our experiments in Sec. 4 indicate that this choice is suitable for indoor relative pose estimation.

4. Experiments

4.1. Datasets

In each of the following experiments, we train our network on either the 7Scenes [24] or Scannet [18] indoor datasets or on the Map-Free [3] outdoor dataset. We evaluate our method on the 7Scenes and Scannet for the indoor case and for the outdoor on the Map-Free and Cambridge landmarks [30] datasets. See the supplementary material for how the GT relative pose is computed.

7Scenes [24]. The Microsoft 7Scenes dataset is a widely used indoor dataset for visual relocalization that contains RGB-D images covering seven different indoor locations (rooms) scanned with KinectFusion. Each scene is provided with training and testing image sequences. We use the dataset as provided in [31, 37], consisting of roughly 40K pairs of images and 80K test pairs.

Cambridge Landmarks [30]. An urban localization dataset capturing four outdoor scenes in Cambridge, UK. The ground truth poses are determined using a standard SfM method (with positions recovered up to an unknown global scale). The images were captured at different times, affected by different lighting and weather condition and containing moving objects including vehicles and pedestrians.

Scannet [18] Scannet is a huge indoor dataset consisting of 1613 monocular sequences with ground truth poses and depth maps. This dataset contains image pairs with wide baselines and extensive texture-less regions. We use the same train/test split used by LoFTR [53], where we sample 200 pairs per scene. This results in 299,200 training pairs (that change in training at each epoch).

Map-Free [3] The Map-free benchmark is a large outdoor dataset consisting of 655 places of interest including sculptures, murals and fountains collected worldwide, such that a place can be well-captured by a single image. Each space comes with a single reference image that serves as the relocalization anchor; all the others are query images with metric poses. This is an extremely challenging setting with limited overlap between image pairs, illumination changes,

Scene/Method	RelPoseNet[31]	8Point[47]	RPR [$q + t$][3]	Ours
Chess	26.0/51.5/8.14	12.3/27.2/3.38	15.4/41.6/5.84	9.1/19.9/3.84
Fire	38.2/70.2/12.3	27.0/46.2/7.82	33.4/69.5/12.2	13.6/22.8/5.09
Heads	23.3/62.0/12.4	17.2/53.0/10.4	19.1/58.5/12.5	9.1/23.6/5.77
Office	30.7/53.0/9.04	18.1/29.6/4.06	23.7/44.6/7.32	11.2/16.6/3.79
Pumpkin	35.1/44.5/9.36	18.7/26.1/3.68	26.9/36.9/6.65	13.9/19.7/3.66
Red Kitchen	40.7/70.7/9.63	21.0/39.3/4.15	26.7/51.3/7.09	12.7/19.1/3.62
Stairs	36.7/77.3/12.2	26.3/50.4/5.02	31.3/62.9/10.2	26.5/44.2/6.05
Average	32.9/61.3/10.4	21.4/38.8/5.49	26.8/59.8/8.83	13.7/23.7/4.55

Table 1. **7Scenes experiment.** The table shows the result of training and testing on the full 7Scenes dataset with the train and test split specified in the dataset. Each entry shows position error in centimeters (left), position angular error in degrees (middle), and orientation error in degrees (right).

and different camera intrinsics between sequences as can be seen in Fig 3. The training set consists of 460 training scenes, 65 validation scenes, and 130 testing scenes.

4.2. Baselines

We compare our approach to three recent end-to-end RPR methods described below. For implementation and training details see the supplementary material.

RelPoseNet [31]. This method uses ResNet34 classification network pre-trained on Imagenet dataset to extract a feature vector for each image. The two vectors are then concatenated and fed into a MLP that regresses the relative pose.

8-Point [47]. This method produces, given an image, a feature embedding using a pre-trained Res-Net18 [27] followed by ViT-tiny [20], a bi-linear cross-attention layer (that considers, for each image, features from the other image), and a quadratic positional encoding. An MLP is finally used to regress the relative position and orientation.

Map-free RPR. This method is taken from the baselines suggested in [3]. It uses a residual UNet (ResUNet) architecture to produce a feature map for each image. A soft feature matching is obtained by computing a 4D correlation volume followed by softmax. This soft matching is then used to warp the features of one image into their corresponding locations in the other image. A regression module is finally used to estimate the relative pose. This method uses no pre-trained components.

We tested the Map-free model in three variants. For the first variant, denoted here as RPR [$q + t$], we retrained the network from scratch to output rotation quaternion and scaled translation parameters. For the second and third variants, we used the model pre-trained on the large Scannet dataset using the 3D-3D and Discretized output methods (denoted as RPR [3D-3D] and RPR disc. respectively) described in [3].

4.3. Metrics and Evaluation

For each method, we measure the position error defined as the Euclidean distance between the predicted and ground truth camera centers.

$$t_{euc\ err}(\mathbf{t}, \hat{\mathbf{t}}) = \|\hat{\mathbf{t}} - \mathbf{t}\|_2 \quad (8)$$

as well as the angle (in degrees) between the predicted and ground truth directions of the camera center vectors

$$t_{ang\ err}(\mathbf{t}, \hat{\mathbf{t}}) = \frac{180}{\pi} \arccos \left(\frac{\hat{\mathbf{t}}^T \mathbf{t}}{\|\hat{\mathbf{t}}\| \|\mathbf{t}\|} \right). \quad (9)$$

We measure orientation error by the angle between the predicted and ground truth orientations, represented in quaternions

$$R_{err}(\mathbf{q}, \hat{\mathbf{q}}) = 2 \arccos \left(\frac{|\hat{\mathbf{q}}^T \mathbf{q}|}{\|\hat{\mathbf{q}}\|} \right). \quad (10)$$

For all measures, we report the median error over the different input pairs. For experiments on Scannet, we also report the AUC for the translation and rotation angular errors.

4.4. Results

7Scenes \rightarrow 7Scenes. In our first experiment, we trained and tested all methods on the 7Scenes dataset. The results are shown in Table 1. Our method (marked as "Ours" in the tables) outperforms the other methods in almost all of the tested scenes, achieving a noticeable improvement in the translation (both Euclidean distance and angular distance) and a smaller advantage over 8Point [47] in the rotation error. Overall, on average, we improve the position prediction by almost 8cm, the position direction prediction by 15°, and the rotation prediction by 1°.

Six scenes \rightarrow 7th scene. The next experiment tests cross-scene generalization. For this experiment, we trained the methods on six of the seven scenes in the 7Scenes dataset and tested them on the remaining scene. We repeated this experiment seven times, each time holding out a different

Scene/Method	RelPoseNet[31]	8Point[47]	RPR [$q + t$][3]	Ours
Chess	22.8/48.2/7.13	27.9/79.6/8.77	27.4/83.5/10.2	18.25/36.72/5.48
Fire	37.4/67.1/19.4	40.6/93.6/12.2	34.0/75.0/13.0	19.94/32.2/7.78
Heads	26.5/69.4/12.8	28.0/79.8/10.7	25.8/83.4/14.0	15.23/25.92/6.36
Office	28.4/54.5/9.63	35.2/81.1/8.84	34.8/79.5/11.2	18.06/27.14/4.99
Pumpkin	34.9/47.4/10.3	42.3/88.5/9.77	36.9/69.4/10.9	23.66/35.29/5.3
Red Kitchen	39.0/69.1/9.73	32.7/74.7/10.3	34.2/81.2/11.7	18.22/26.37/5.15
Stairs	45.6/67.2/12.7	36.8/79.3/8.98	37.0/96.6/11.7	28.6/47.3/8.04
Average	33.5/60.4/11.7	34.8/82.4/9.94	32.9/81.2/11.8	20.2/33.0/6.16

Table 2. **Six Scenes experiment.** The table shows the result of training on six scenes from the 7Scenes dataset and testing on the remaining scene. Each entry shows position error in centimeters (left), position angular error in degrees (middle), and orientation error in degrees (right).

Method	All Keyframes		2 Keyframes		1 Keyframe	
	Error↓	Prec.(25 cm, 5°)↑	Error↓	Prec.(25 cm, 5°)↑	Error↓	Prec.(25 cm, 5°)↑
DSAC*(single scene)[12]	3 cm, 1.1°	0.97	31 cm, 7.4°	0.41	77 cm, 25.5°	0.22
LoFTR[53]+5Pt+Depth Scale	12 cm, 1.7°	0.83	29 cm, 2.8°	0.50	33 cm, 6.4°	0.38
SG[50]+5Pt+Depth Scale	13 cm, 1.8°	0.81	26 cm, 3.3°	0.51	30 cm, 5.4°	0.37
SIFT[36]+5Pt+Depth Scale	16 cm, 2.5°	0.74	41 cm, 7.1°	0.37	60 cm, 23.7°	0.24
RPR [3D-3D][3]	16 cm, 4.5°	0.60	42 cm, 8.3°	0.18	66 cm, 12.8°	0.11
RPR [3D - 3D] f.t. hard [3]	17 cm, 4.2°	0.61	37 cm, 7.3°	0.20	50 cm, 10.8°	0.13
RPR disc.[3]	18 cm, 4.9°	0.53	51 cm, 10.0°	0.12	67 cm, 15.9°	0.07
Ours	11 cm, 3.2°	0.73	35 cm, 6.86°	0.27	46 cm, 11.1°	0.16

Table 3. **7scenes relocation.** The table shows the result of training on Scannet and testing on the 7Scenes test set for relocation using 1,2 or all the mapped reference frames. The errors are the average of the median error over all the scenes. "RPR [3D-3D] f.t. hard" refers to the [3D-3D] network in [3], fine-tuned over Scannet image pairs with a small overlap. DSAC* is a single scene absolute pose regression network. For this experiment, we also report the precision (Prec.) at the position error of 25 cm, and rotation error of 5°. We use **blue** to indicate the best result among the RPR methods, and **orange** to indicate the best result among the feature matching methods.

scene. Results are shown in Table 2. Our method outperforms all other methods in this scenario as well. Notice in particular the advantage in the position angular error, as both 8Point and RPR [$q + t$] obtain a near random average median angular error (larger than 80°). Overall, on average, relative to the best existing method, we improve the position prediction by 12cm, the position direction prediction by 27°, and the rotation prediction by 3.7°.

Scannet → 7Scenes. The third experiment tests cross-dataset generalization. Here all methods are trained on the Scannet dataset and tested on the 7Scenes test set for the relocation task. In this task, we evaluate the methods for relocation with a query image against either a single keyframe, two keyframes, or all keyframes. The single keyframe case is equivalent to the relative pose regression task. In the two/all keyframes case, we first select one of the two/all keyframes whose distance in the DenseVLAD [54] feature space to the query image is smaller and then perform RPR on the query and the selected keyframe. The split is taken from [3]. Results are shown in Table 3. Our method outperforms all other RPR methods, improving both translation (metric and angular) and rotation errors (with the

exception of the finetuned RPR [3D-3D], which achieves a slight rotation advantage in the single keyframe case.). Nevertheless, while our method achieves significantly better performance than SIFT [36], its performance is still surpassed by learnable feature matching methods [50, 53] combined with a depth estimation method [35], for obtaining the metric scale from the depth as explained in [3].

Scannet → Scannet. We also evaluate our methods on the Scannet-1500 test set for further cross-scene evaluation. As seen in Table 4, our method improves over the baselines with a large margin in both the angular AUC@5°/10°/20° and the median translation euclidean error and yields an improvement in the median rotation error. As in the previous experiment, our method surpasses SIFT [36], but achieves inferior results compared to [50, 53] combined with a depth estimation method [43].

Across Indoor → Outdoor Datasets. For this experiment we wanted to test our model’s ability to generalize from indoor training to outdoor scenes. For that, we test models that were trained on 7Scenes or Scannet on the Cambridge Landmarks dataset [30]. Since there are major scale differences between indoor to outdoor scenes, and the GT poses

Method	Trans. AUC \uparrow			Rot. AUC \uparrow			Pose median errors \downarrow	
	@ 5 $^\circ$	@10 $^\circ$	@20 $^\circ$	@ 5 $^\circ$	@10 $^\circ$	@20 $^\circ$	Trans cm	Rotation $^\circ$
LoFTR[53]+5Pt+Depth Scale	23.4	42.4	60.6	52.6	69.1	79.7	13	1.8
SG[50]+5Pt+Depth Scale	18.2	35.6	54.7	43.5	62.0	75.4	15	2.4
SIFT[36]+5Pt+Depth Scale	6.5	14.7	26.3	24.4	36.3	47.1	38	8.0
RPR [3D-3D][3]	4.5	13.6	31.8	28.1	48.6	65.9	20	4.1
RPR disc.[3]	3.6	11.4	29.7	25.3	44.8	62.4	22	4.7
Ours	6.4	18.8	40.0	33.3	54.0	70.5	15	3.4

Table 4. **Scannet experiment.** The table shows the result of training on Scannet and testing on the Scannet-1500 test set. We use **blue** to indicate the best result among the RPR methods, and **orange** to indicate the best result among the feature matching methods.



Figure 3. A pair of images from the Map-Free test set. There is little overlap and a significant change in the color intensities, probably due to a time difference between the images.

were acquired by SFM, making the positions recovered up to an unknown global scale, we report only angular error for this experiment. Results are shown in Table 5. When trained on 7Scenes, our method outperforms all other methods by over 25 $^\circ$ in translation direction and nearly 1 $^\circ$ better in rotation compared to the second-best method 8Point. Unfortunately, all the methods that were trained on 7Scenes generalize poorly to outdoor. When trained on Scannet our method outperforms RPR [3D-3D] by 6 $^\circ$ /0.3 $^\circ$ on translation and rotation, respectively. Overall, our method outperforms all other tested methods in this scenario.

Limitations. Pose regression with our method depends on obtaining a reasonable warping of the LoFTR feature maps for the two input images. This may be difficult to achieve when input image pairs are captured under wide baseline conditions or from extreme viewing directions. This appears to be the case in the Map-free dataset, in which many of the image pairs are very partially overlapping and a significant number have no overlap at all, see [3], Fig. 5 therein and the example in Fig. 3. Table 6 shows the result of training and testing our network on this dataset, compared to various baselines including end-to-end RPR methods and RANSAC-based methods. Our method’s results are not as

good as theirs and probably are further hurt because our LoFTR encoder is fixed and not trained on this dataset.

Inference time. Table 8 shows inference time for the different methods. Feature matching models have substantially slower inference times compared to regression-based relative pose models, particularly when combined with a depth prediction model for scale estimation

4.5. Ablations

We ablate our choice of backbone, disentanglement of the regression heads, and the warping mechanism.

Backbone. For the backbone, we compare the use of LoFTR to Dino-ViT [16] and the ACE encoder [14]. Dino-ViT is a self-supervised vision transformer whose features were shown to capture a strong structural and semantic representation [2, 58]. In our experiment, we concatenated the class token to all patch tokens from the output of the last transformer blocks and pass those to our matching and warping model. The ACE encoder is a convolutional NN with the same architecture as the DSAC* encoder [59]. The encoder is trained on 100 scans from Scannet dataset, and it is attached to regression heads that are trained on individual scenes, using the DSAC* framework. As [14] shows, the resulting network serves as a scene-agnostic descriptor for visual relocalization.

Loss and network architecture. We compared our proposed loss (7) with one in which we drop the cosine similarity term $\mathcal{L}_{\text{dir}}(I_A, I_B)$. We further added balancing weights and learned them as in [29]. Additionally, we tested models with two and three heads. Using additional regression heads increases the number of parameters but eliminates balancing weights (since the backbone is pre-trained). Finally, we compared utilizing soft to hard warping in our model.

We trained and tested our ablated method on the Scannet dataset. Results are shown in Table 7. The best results are obtained with the LoFTR backbone, hard warping, and a single head with unit balancing weights. Utilizing three heads produced nearly similar results. Replacing LoFTR with either DINO-ViT or ACE yielded significant degradation, justifying our use of LoFTR, an IM model, as the

Scene/Method	RelPoseNet[31]	8Point[47]	RPR [q + t][3]	Ours	RPR [3D-3D][3]-Scannet	Ours-Scannet
KingsCollege	86.0/18.62	90.4/7.889	94.8/8.71	45.7/6.20	31.2/ 4.25	27.0/4.39
OldHospital	91.0/18.23	87.3/9.674	86.9/12.06	62.1/10.01	36.3/6.31	28.1/5.51
ShopFacade	88.9/19.36	88.9/11.46	81.9/14.42	37.8/10.27	21.6/ 6.68	17.1/7.29
StMarysChurch	92.2/20.15	89.9/12.59	85.1/14.17	51.9/12.09	29.8/7.29	21.9/6.25
Average	89.5/19.09	89.1/10.40	87.1/15.01	60.6/9.64	29.7/6.13	23.5/5.86

Table 5. **Cambridge Landmarks experiment.** The table shows the result of training on 7scenes/Scannet datasets and testing on the Cambridge outdoors dataset. Each entry shows position angular error in degrees (left), and orientation error in degrees (right).

Method	Precision (VCRE < 90px) \uparrow	Median Reproj. Error (px) \downarrow	Precision (Err < 25 cm, 5 $^\circ$) \uparrow	Median Trans. Error (m) \downarrow	Median Rot. Error ($^\circ$) \downarrow
LoFTR[53]+5Pt+Depth Scale	34.7%	167.6	15.4%	1.98	30.5
SG[50]+5Pt+Depth Scale	36.1%	160.3	16.8%	1.88	25.4
SIFT[36]+5Pt+Depth Scale	25.0%	222.8	10.3%	2.93	61.4
RPR[R(6 D)+t][3]	40.2%	147.1	6.0%	1.68	22.5
RPR [3D-3D][3]	38.7%	148.7	6.0%	1.69	22.9
RPR disc.[3]	35.4%	166.3	10.5%	1.83	23.2
Ours	35.6%	155.3	6.9%	2.00	25.8

Table 6. **Map-Free dataset experiment.** The table shows the result of training and testing on the Map-Free dataset. The depth is predicted by DPT [43] a monocular depth network, its output is utilized to calculate the scale for image matching-based methods as explained in [3]. Virtual Correspondence Reprojection Error (VCRE) is the average Euclidean reprojection error of virtual 3D-2D correspondences.

Experiment	Method	Pose estimation AUC \uparrow			Pose median errors \downarrow		
		@ 5 $^\circ$	@10 $^\circ$	@20 $^\circ$	trans cm	trans $^\circ$	rotation $^\circ$
Backbone	Dino[16]	2.0	8.2	23.7	23	17.7	4.28
	ACE[14]	1.7	9.1	25.6	20	15.6	4.58
Warping	Soft Warping	3.6	14.9	35.7	16	11.6	3.5
Loss & Architecture	Single head (\mathbf{q}, \mathbf{t})	3.6	15.0	35.8	16	11.4	3.5
	Single head (\mathbf{q}, \mathbf{t}) w/o cosine similarity	3.5	13.6	31.9	18	13.4	3.77
	Two heads ($(\mathbf{q}), (\mathbf{t})$)	3.0	12.6	32.3	17	13.0	3.27
	Two heads ($\mathbf{q}, (\mathbf{t}_{dir}, \mathbf{s})$)	3.2	13.6	33.7	16	12.4	3.07
	Three heads ($(\mathbf{q}), (\mathbf{t}_{dir}), (\mathbf{s})$)	3.5	14.6	35.7	16	11.7	3.11
	Single head ($\mathbf{q}, \mathbf{t}_{dir}, \mathbf{s}$)	3.8	15.4	36.4	15	11.1	3.40

Table 7. **Ablation experiment.** The table shows the result of training on Scannet and testing on the Scannet-1500 test set. With the train and test split specified in the text. Following this ablation we use single-headed architecture with a LoFTR backbone and hard warping.

backbone.

Time [ms]	LoFTR	SuperGlue	RPR [3D-3D]	Ours
Method	79	71	21	26
+ Depth estimation	40	40	-	-
Total time	119	111	21	26

Table 8. **Inference time.** Feature matching models are significantly slower than regression-based relative pose models in terms of inference time.

5. Conclusion

This paper proposes to use image matching as a pre-training task to learn better feature representations toward a generalizable end-to-end neural network for relative pose regression. Our method relies on a semi-dense feature map produced by a pre-trained LoFTR network, image warping and pose regressor. We showed that this architecture, coupled

with a loss function that separates the translation direction and scale, achieves improved results on various datasets and in cross-scene and cross-dataset problems. Our method has effectively reduced the performance gap between RPRs and feature matching models while maintaining significantly faster inference speeds. We also showed limitations in handling image pairs in wide baseline and sharp illumination changes. We plan to continue exploring network architectures to further improve the accuracy of RPR networks.

Acknowledgments

Research at the Weizmann Institute was partially supported by the Israel Science Foundation, grant No. 1639/19, by the Israeli Council for Higher Education (CHE) via the Weizmann Data Science Research Center, by the MBZUAI-WIS Joint Program for Artificial Intelligence Research and from the Estates of Tully and Michele Plesser and the Anita James Rosen and Harry Schutzman Foundations.

References

- [1] Yehya Abouelnaga, Mai Bui, and Slobodan Ilic. Distill-pose: Lightweight camera localization using auxiliary learning. In *2021 IEEE/RISJ International Conference on Intelligent Robots and Systems (IROS)*, pages 7919–7924. IEEE, 2021. [3](#)
- [2] Shir Amir, Yossi Gandelsman, Shai Bagon, and Tali Dekel. Deep vit features as dense visual descriptors. *ECCVW What is Motion For?*, 2022. [7](#)
- [3] Eduardo Arnold, Jamie Wynn, Sara Vicente, Guillermo Garcia-Hernando, Áron Monszpart, Victor Adrian Prisacariu, Daniyar Turmukhambetov, and Eric Brachmann. Map-free visual relocalization: Metric pose relative to a single image. In *ECCV*, 2022. [1](#), [2](#), [3](#), [4](#), [5](#), [6](#), [7](#), [8](#)
- [4] Vassileios Balntas, Shuda Li, and Victor Prisacariu. Relocnet: Continuous metric learning relocalisation using neural nets. In *Proceedings of the European Conference on Computer Vision (ECCV)*, pages 751–767, 2018. [3](#)
- [5] Daniel Barath, Jiri Matas, and Jana Noskova. Magsac: marginalizing sample consensus. In *Proceedings of the IEEE/CVF Conference on Computer Vision and Pattern Recognition*, pages 10197–10205, 2019. [2](#)
- [6] Daniel Barath, Jana Noskova, Maksym Ivashechkin, and Jiri Matas. Magsac++, a fast, reliable and accurate robust estimator. In *Proceedings of the IEEE/CVF conference on computer vision and pattern recognition*, pages 1304–1312, 2020. [1](#), [2](#)
- [7] Axel Barroso-Laguna, Eric Brachmann, Victor Prisacariu, Gabriel Brostow, and Daniyar Turmukhambetov. Two-view geometry scoring without correspondences. In *Proceedings of the IEEE/CVF Conference on Computer Vision and Pattern Recognition*, 2023. [1](#)
- [8] Herbert Bay, Tinne Tuytelaars, and Luc Van Gool. Surf: Speeded up robust features. In *European conference on computer vision*, pages 404–417. Springer, 2006. [1](#), [2](#)
- [9] Aritra Bhowmik, Stefan Gumhold, Carsten Rother, and Eric Brachmann. Reinforced feature points: Optimizing feature detection and description for a high-level task. In *Proceedings of the IEEE/CVF conference on computer vision and pattern recognition*, pages 4948–4957, 2020. [2](#)
- [10] Eric Brachmann and Carsten Rother. Expert sample consensus applied to camera re-localization. In *Proceedings of the IEEE/CVF International Conference on Computer Vision*, pages 7525–7534, 2019. [3](#)
- [11] Eric Brachmann and Carsten Rother. Neural-guided ransac: Learning where to sample model hypotheses. In *Proceedings of the IEEE/CVF International Conference on Computer Vision*, pages 4322–4331, 2019. [3](#)
- [12] Eric Brachmann and Carsten Rother. Visual camera relocalization from rgb and rgb-d images using dsac. *IEEE transactions on pattern analysis and machine intelligence*, 44(9):5847–5865, 2021. [6](#)
- [13] Eric Brachmann, Alexander Krull, Sebastian Nowozin, Jamie Shotton, Frank Michel, Stefan Gumhold, and Carsten Rother. Dsac-differentiable ransac for camera localization. In *Proceedings of the IEEE conference on computer vision and pattern recognition*, pages 6684–6692, 2017. [3](#)
- [14] Eric Brachmann, Tommaso Cavallari, and Victor Adrian Prisacariu. Accelerated coordinate encoding: Learning to relocalize in minutes using rgb and poses. In *CVPR*, 2023. [3](#), [7](#), [8](#)
- [15] Michael Calonder, Vincent Lepetit, Christoph Strecha, and Pascal Fua. Brief: Binary robust independent elementary features. In *European conference on computer vision*, pages 778–792. Springer, 2010. [1](#), [2](#)
- [16] Mathilde Caron, Hugo Touvron, Ishan Misra, Hervé Jégou, Julien Mairal, Piotr Bojanowski, and Armand Joulin. Emerging properties in self-supervised vision transformers. In *Proceedings of the International Conference on Computer Vision (ICCV)*, 2021. [7](#), [8](#)
- [17] Christopher Choy, Junha Lee, René Ranftl, Jaesik Park, and Vladlen Koltun. High-dimensional convolutional networks for geometric pattern recognition. In *Proceedings of the IEEE/CVF conference on computer vision and pattern recognition*, pages 11227–11236, 2020. [3](#)
- [18] Angela Dai, Angel X Chang, Manolis Savva, Maciej Halber, Thomas Funkhouser, and Matthias Nießner. Scannet: Richly-annotated 3d reconstructions of indoor scenes. In *Proceedings of the IEEE conference on computer vision and pattern recognition*, pages 5828–5839, 2017. [3](#), [4](#)
- [19] Daniel DeTone, Tomasz Malisiewicz, and Andrew Rabinovich. Superpoint: Self-supervised interest point detection and description. In *Proceedings of the IEEE conference on computer vision and pattern recognition workshops*, pages 224–236, 2018. [2](#)
- [20] Alexey Dosovitskiy, Lucas Beyer, Alexander Kolesnikov, Dirk Weissenborn, Xiaohua Zhai, Thomas Unterthiner, Mostafa Dehghani, Matthias Minderer, Georg Heigold, Sylvain Gelly, et al. An image is worth 16x16 words: Transformers for image recognition at scale. *arXiv preprint arXiv:2010.11929*, 2020. [3](#), [5](#)
- [21] Mihai Dusmanu, Ignacio Rocco, Tomas Pajdla, Marc Pollefeys, Josef Sivic, Akihiko Torii, and Torsten Sattler. D2-net: A trainable cnn for joint description and detection of local features. In *Proceedings of the IEEE/CVF conference on computer vision and pattern recognition*, pages 8092–8101, 2019. [2](#)
- [22] Sovann En, Alexis Lechervy, and Frédéric Jurie. Rpnnet: An end-to-end network for relative camera pose estimation. In *Proceedings of the European Conference on Computer Vision (ECCV) Workshops*, pages 0–0, 2018. [3](#)
- [23] Martin A Fischler and Robert C Bolles. Random sample consensus: a paradigm for model fitting with applications to image analysis and automated cartography. *Communications of the ACM*, 24(6):381–395, 1981. [1](#), [2](#)
- [24] Ben Glocker, Shahram Izadi, Jamie Shotton, and Antonio Criminisi. Real-time rgb-d camera relocalization. In *2013 IEEE International Symposium on Mixed and Augmented Reality (ISMAR)*, pages 173–179. IEEE, 2013. [4](#), [12](#)
- [25] Richard Hartley and Andrew Zisserman. *Multiple view geometry in computer vision*. Cambridge university press, 2003. [2](#)
- [26] Richard I Hartley. In defense of the eight-point algorithm. *IEEE Transactions on pattern analysis and machine intelligence*, 19(6):580–593, 1997. [3](#)

- [27] Kaiming He, Xiangyu Zhang, Shaoqing Ren, and Jian Sun. Deep residual learning for image recognition. In *Proceedings of the IEEE conference on computer vision and pattern recognition*, pages 770–778, 2016. 5
- [28] Wei Jiang, Eduard Trulls, Jan Hosang, Andrea Tagliasacchi, and Kwang Moo Yi. COTR: Correspondence transformer for matching across images. In *Proceedings of the IEEE/CVF International Conference on Computer Vision*, pages 6207–6217, 2021. 2
- [29] Alex Kendall and Roberto Cipolla. Geometric loss functions for camera pose regression with deep learning. In *Proceedings of the IEEE conference on computer vision and pattern recognition*, pages 5974–5983, 2017. 1, 4, 7
- [30] Alex Kendall, Matthew Grimes, and Roberto Cipolla. Posenet: A convolutional network for real-time 6-dof camera relocalization. In *Proceedings of the IEEE international conference on computer vision*, pages 2938–2946, 2015. 1, 4, 6
- [31] Zakaria Laskar, Iaroslav Melekhov, Surya Kalia, and Juho Kannala. Camera relocalization by computing pairwise relative poses using convolutional neural network. In *Proceedings of the IEEE International Conference on Computer Vision Workshops*, pages 929–938, 2017. 1, 3, 4, 5, 6, 8, 12
- [32] Amy Lin, Jason Y Zhang, Deva Ramanan, and Shubham Tulsiani. Relpose++: Recovering 6d poses from sparse-view observations. *arXiv preprint arXiv:2305.04926*, 2023. 3
- [33] Tsung-Yi Lin, Piotr Dollár, Ross Girshick, Kaiming He, Bharath Hariharan, and Serge Belongie. Feature pyramid networks for object detection. In *Proceedings of the IEEE conference on computer vision and pattern recognition*, pages 2117–2125, 2017. 3
- [34] Philipp Lindenberger, Paul-Edouard Sarlin, and Marc Pollefeys. LightGlue: Local Feature Matching at Light Speed. In *ICCV*, 2023. 2
- [35] Chen Liu, Kihwan Kim, Jinwei Gu, Yasutaka Furukawa, and Jan Kautz. PlanerCNN: 3d plane detection and reconstruction from a single image. In *Proceedings of the IEEE/CVF Conference on Computer Vision and Pattern Recognition*, pages 4450–4459, 2019. 6
- [36] David G Lowe. Distinctive image features from scale-invariant keypoints. *International journal of computer vision*, 60(2):91–110, 2004. 1, 2, 6, 7, 8
- [37] Iaroslav Melekhov, Juha Ylioinas, Juho Kannala, and Esa Rahtu. Relative camera pose estimation using convolutional neural networks. In *International Conference on Advanced Concepts for Intelligent Vision Systems*, pages 675–687. Springer, 2017. 3, 4
- [38] David Nistér. An efficient solution to the five-point relative pose problem. *IEEE transactions on pattern analysis and machine intelligence*, 26(6):756–770, 2004. 2
- [39] Onur Özyeşil, Vladislav Voroninski, Ronen Basri, and Amit Singer. A survey of structure from motion*. *Acta Numerica*, 26:305–364, 2017. 1
- [40] Adam Paszke, Sam Gross, Francisco Massa, Adam Lerer, James Bradbury, Gregory Chanan, Trevor Killeen, Zeming Lin, Natalia Gimelshein, Luca Antiga, et al. Pytorch: An imperative style, high-performance deep learning library. *Advances in neural information processing systems*, 32, 2019. 12
- [41] Rahul Raguram, Jan-Michael Frahm, and Marc Pollefeys. A comparative analysis of ransac techniques leading to adaptive real-time random sample consensus. In *European conference on computer vision*, pages 500–513. Springer, 2008. 2
- [42] René Ranftl and Vladlen Koltun. Deep fundamental matrix estimation. In *Proceedings of the European conference on computer vision (ECCV)*, pages 284–299, 2018. 3
- [43] René Ranftl, Alexey Bochkovskiy, and Vladlen Koltun. Vision transformers for dense prediction. In *Proceedings of the IEEE/CVF international conference on computer vision*, pages 12179–12188, 2021. 6, 8
- [44] Jeremy Reizenstein, Roman Shapovalov, Philipp Henzler, Luca Sbordone, Patrick Labatut, and David Novotny. Common objects in 3d: Large-scale learning and evaluation of real-life 3d category reconstruction. In *Proceedings of the IEEE/CVF International Conference on Computer Vision*, pages 10901–10911, 2021. 3
- [45] Jerome Revaud, Cesar De Souza, Martin Humenberger, and Philippe Weinzaepfel. R2d2: Reliable and repeatable detector and descriptor. *Advances in neural information processing systems*, 32, 2019. 2
- [46] Edgar Riba, Dmytro Mishkin, Daniel Ponsa, Ethan Rublee, and Gary Bradski. Kornia: an open source differentiable computer vision library for pytorch. In *Proceedings of the IEEE/CVF Winter Conference on Applications of Computer Vision*, pages 3674–3683, 2020. 12
- [47] Chris Rockwell, Justin Johnson, and David F Fouhey. The 8-point algorithm as an inductive bias for relative pose prediction by ViTs. *arXiv preprint arXiv:2208.08988*, 2022. 1, 3, 5, 6, 8
- [48] Edward Rosten and Tom Drummond. Machine learning for high-speed corner detection. In *European conference on computer vision*, pages 430–443. Springer, 2006. 1, 2
- [49] Ethan Rublee, Vincent Rabaud, Kurt Konolige, and Gary Bradski. Orb: An efficient alternative to sift or surf. In *2011 International conference on computer vision*, pages 2564–2571. Ieee, 2011. 1, 2
- [50] Paul-Edouard Sarlin, Daniel DeTone, Tomasz Malisiewicz, and Andrew Rabinovich. SuperGlue: Learning feature matching with graph neural networks. In *CVPR*, 2020. 2, 6, 7, 8
- [51] Johannes Lutz Schönberger and Jan-Michael Frahm. Structure-from-motion revisited. In *Conference on Computer Vision and Pattern Recognition (CVPR)*, 2016. 1
- [52] Noah Snavely, Steven M Seitz, and Richard Szeliski. Photo tourism: exploring photo collections in 3d. In *ACM siggraph 2006 papers*, pages 835–846. 2006. 1
- [53] Jiaming Sun, Zehong Shen, Yuang Wang, Hujun Bao, and Xiaowei Zhou. LoFTR: Detector-free local feature matching with transformers. *CVPR*, 2021. 1, 2, 3, 4, 6, 7, 8, 12
- [54] Akihiko Torii, Relja Arandjelovic, Josef Sivic, Masatoshi Okutomi, and Tomas Pajdla. 24/7 place recognition by view synthesis. In *Proceedings of the IEEE conference on computer vision and pattern recognition*, pages 1808–1817, 2015. 6

- [55] Prune Truong, Martin Danelljan, Luc V Gool, and Radu Timofte. Gocor: Bringing globally optimized correspondence volumes into your neural network. *Advances in Neural Information Processing Systems*, 33:14278–14290, 2020. 2
- [56] Prune Truong, Martin Danelljan, and Radu Timofte. Glunet: Global-local universal network for dense flow and correspondences. In *Proceedings of the IEEE/CVF conference on computer vision and pattern recognition*, pages 6258–6268, 2020.
- [57] Prune Truong, Martin Danelljan, Luc Van Gool, and Radu Timofte. Learning accurate dense correspondences and when to trust them. In *Proceedings of the IEEE/CVF Conference on Computer Vision and Pattern Recognition*, pages 5714–5724, 2021. 2
- [58] Narek Tumanyan, Omer Bar-Tal, Shai Bagon, and Tali Dekel. Splicing vit features for semantic appearance transfer. In *Proceedings of the IEEE/CVF Conference on Computer Vision and Pattern Recognition*, pages 10748–10757, 2022. 7
- [59] Mehmet Ozgur Turkoglu, Eric Brachmann, Konrad Schindler, Gabriel J Brostow, and Aron Monszpart. Visual camera re-localization using graph neural networks and relative pose supervision. In *2021 International Conference on 3D Vision (3DV)*, pages 145–155. IEEE, 2021. 7
- [60] Michał Tyszkiewicz, Pascal Fua, and Eduard Trulls. Disk: Learning local features with policy gradient. *Advances in Neural Information Processing Systems*, 33:14254–14265, 2020. 2
- [61] Ashish Vaswani, Noam Shazeer, Niki Parmar, Jakob Uszkoreit, Llion Jones, Aidan N Gomez, Łukasz Kaiser, and Illia Polosukhin. Attention is all you need. *Advances in neural information processing systems*, 30, 2017. 3
- [62] Dominik Winkelbauer, Maximilian Denninger, and Rudolph Triebel. Learning to localize in new environments from synthetic training data. In *2021 IEEE International Conference on Robotics and Automation (ICRA)*, pages 5840–5846. IEEE, 2021. 3
- [63] Changchang Wu. Visualsfm: A visual structure from motion system. <http://www.cs.washington.edu/homes/ccwu/vsfm>, 2011. 1
- [64] Changchang Wu. Towards linear-time incremental structure from motion. In *2013 International Conference on 3D Vision-3DV 2013*, pages 127–134. IEEE, 2013. 1
- [65] Kwang Moo Yi, Eduard Trulls, Vincent Lepetit, and Pascal Fua. Lift: Learned invariant feature transform. In *European conference on computer vision*, pages 467–483. Springer, 2016. 2
- [66] Kwang Moo Yi, Eduard Trulls, Yuki Ono, Vincent Lepetit, Mathieu Salzmann, and Pascal Fua. Learning to find good correspondences. In *Proceedings of the IEEE conference on computer vision and pattern recognition*, pages 2666–2674, 2018. 12
- [67] Jason Y Zhang, Deva Ramanan, and Shubham Tulsiani. Rel-pose: Predicting probabilistic relative rotation for single objects in the wild. In *European Conference on Computer Vision*, pages 592–611. Springer, 2022. 3
- [68] Qunjie Zhou, Torsten Sattler, Marc Pollefeys, and Laura Leal-Taixe. To learn or not to learn: Visual localization

from essential matrices. In *2020 IEEE International Conference on Robotics and Automation (ICRA)*, pages 3319–3326. IEEE, 2020. 3

Appendix

A. Implementation Details

Our method is implemented using Pytorch [40] and Kornia [46]. All models are trained and evaluated using the same strategy. In all the experiments, we use the Adam optimizer initialized with the default values $\beta_1 = 0.9$ and $\beta_2 = 0.999$. The models are trained respectively for 80/60 epochs on the 7Scenes/Scannet datasets with an effective batch size of 200. We use a linear decay strategy, where the learning rate is reduced by a factor of 0.9 every 6 epochs, starting with a learning rate of 1×10^{-3} . Using four NVIDIA Tesla A40 GPUs, the training time of our model on the full 7Scenes dataset is roughly 24 hours and on Scannet roughly 72 hours. Using Nvidia V100 GPU the inference time of our model is 26ms. We use early stopping with the validation dataset for all methods to determine the best set of weights.

B. Network Architecture

We reduced the size of the images to size of 256×341 following [31]. Therefore, the feature pyramid network [66] in LoFTR[53] outputs a $256 \times 32 \times 42$ feature map per image. The resolution is preserved through the attention layers. The warping module concatenates the feature maps of matching points in the two images and adds 5 channels, including the coordinates of the two matching points and the matching score. This results in a 2D feature map as output of size $517 \times 32 \times 42$. Which we feed then to a ResNet block, which results in a feature vector of size 1152 (after flattening it). This feature vector we then feed into a three different MLPs which output the predicted translation direction, scale and the orientation.

C. Ground Truth Relative Pose in the 7Scenes Dataset

We note that the relative camera positions in the 7scenes [24] dataset, obtained from RelPoseNet[31], are erroneously set to $\mathbf{t}_i - \mathbf{t}_j$ where $\mathbf{t}_i, \mathbf{t}_j$ represent the absolute position of the i^{th} and j^{th} cameras, instead of $\mathbf{t}_i - R_{ij}^T \mathbf{t}_j$ as it should be, and how it's computed in the other datasets, where R_{ij} denotes the relative orientation between cameras i and j . We rectify this error in our experiments, when we train the different relative pose regression methods on the 7scenes dataset.



Figure 4. **7scenes dataset**. Pairs of images from the 7Scenes dataset, including scenes with repetitive patterns.

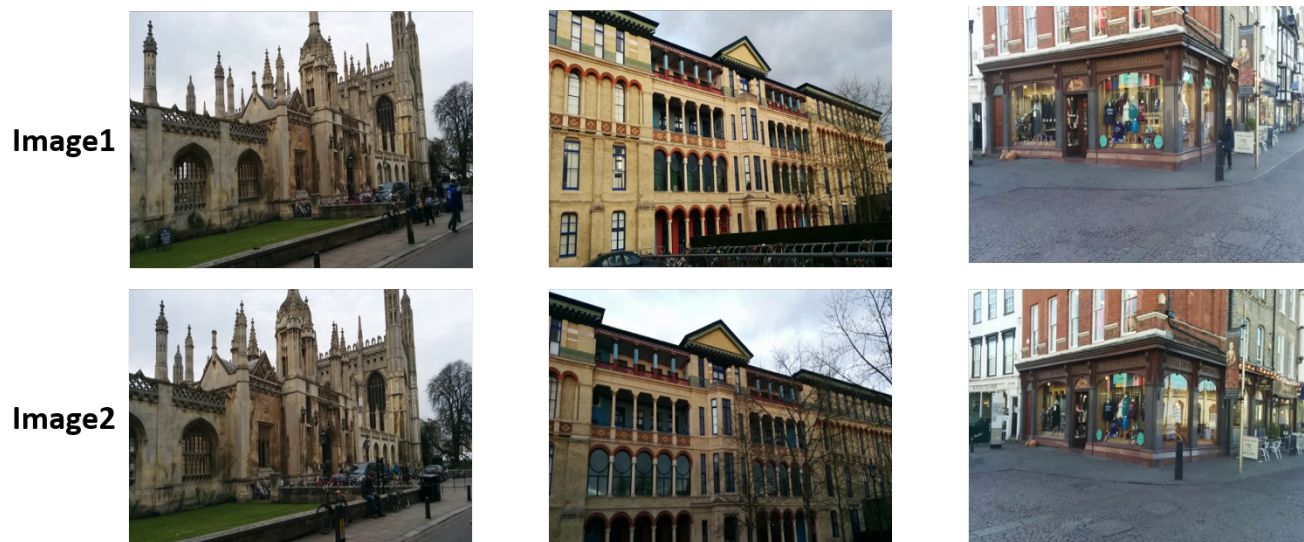


Figure 5. **Cambridge Landmarks dataset**. Pairs of images from the Kings College, Old Hospital and Shop Facade from the Cambridge Landmarks dataset. Notice the different lighting conditions.

Image1



Image2



Figure 6. **Scannet dataset.** Pairs of images from the Scannet dataset, including scenes with repetitive patterns.